water

MDPI

Article

Representative and Morphological Waves along the Adriatic Italian Coast in a Changing Climate

Piero Ruol [1], Luca Martinelli [1,*], Chiara Favaretto [1], Francesco Barbariol [2] and Alvise Benetazzo [2]

[1] Dipartimento di Ingegneria Civile, Edile e Ambientale (ICEA Department), Padua University, Via Ognissanti 39, 35129 Padova, Italy
[2] Istituto di Scienze Marine (ISMAR), Consiglio Nazionale delle Ricerche (CNR), 30122 Venice, Italy
* Correspondence: luca.martinelli@unipd.it

Abstract: This paper investigates the impact of climate change on coastal dynamics along the Adriatic Italian coast, with reference to the period 2021–2050 considering the IPCC RCP 4.5 and 8.5 scenarios. The wave datasets are obtained by forcing a spectral wave model with ERA5 wind fields corrected with a procedure that makes them suitable for the investigated semi-enclosed basin where local meteorological events occur at scales of a few kilometers. The wave climate changes between the historic run (1981–2010) and the future scenarios are studied in terms of mean values, percentile and extreme waves in 120 virtual buoys along the coasts. Moreover, a morphological equivalent wave is computed for all the datasets to highlight the consequences of climate change on coastal sediment transport. Along the Adriatic Italian coast, a small decrease in the significant wave heights is found, both for mean and extreme values, and the sediment transport is reduced. However, significant deviations along the coast are highlighted and the longshore sediment transport even reverses its direction in some locations for the future scenarios.

Keywords: wave climate; WaveWatch III; coastal sediment transport; IPCC scenarios

Citation: Ruol, P.; Martinelli, L.; Favaretto, C.; Barbariol, F.; Benetazzo, A. Representative and Morphological Waves along the Adriatic Italian Coast in a Changing Climate. *Water* **2022**, *14*, 2678. https://doi.org/10.3390/w14172678

Academic Editors: Marcello Di Risio and Francesco Aristodemo

Received: 20 July 2022
Accepted: 25 August 2022
Published: 29 August 2022

1. Introduction

For long-term coastal management, predictions of the influence of climate change in the littoral zone is of paramount importance. Among the relevant aspects of interest, there are wave statistics close to the shoreline and longshore sediment transport. This paper investigates these predicted climate change effects for the Adriatic Italian coast, capitalizing on a previous study (Benetazzo et al. [1]) that modeled the waves in the Adriatic Sea.

Several studies have been carried out to investigate the climate change effect on wave statistics in the Adriatic Sea or more in generally in the Mediterranean Sea, based on wave hindcast or future projections, and most of them agree in suggesting a lower storminess for the future scenarios. Benetazzo et al. [2] highlight an overall decrease in sea severity with reference to the A1B intermediate emissions scenario (older IPCC report [3]) for the period 2070–2099. The authors found that this decrease is mostly due to a reduction in cyclonic activity in the central Mediterranean basin, and the variation appears more remarkable in the offshore regions and progressively less relevant towards the coast. Denamiel et al. [4] found that, during extreme events, the significant wave heights and peak periods relative to 2060–2100 under the RCP 4.5 and RCP 8.5 scenarios are likely to decrease compared to the 1979–2019 period. De Leo et al. [5] performed an analysis of wave climate changes under emission scenario RCP 8.5 for the period 2006–2100, over the entire Mediterranean basin. Their analysis revealed that the wave climate of the Mediterranean Sea will be mainly characterized by downward trends of significant wave height and mean period, while the wave directions may be characterized by a slight eastward shift. Unlike the studies mentioned above, Barbariol et al. [6], analyzing a 40-year (1980–2019) wave hindcast in the Mediterranean Sea, found that the typical and extreme significant wave heights and the

maximum individual wave heights are decreasing during summer and increasing during winter. Similarly, Caloiero et al. [7,8] showed a general increase in wave storminess at an annual scale, mainly detected in the Algerian and Ionian seas, analyzing a 40-year-long hindcast time series (1979–2018).

Few studies on the effect of climate change address the coastal sediment transport modification. Grases et al. [9] analyzed through a modeling chain the future evolution of erosion hazards at the Ebro Delta and found that longshore sediment transport processes are slowed down, while they are enhanced in the cross-shore direction. Bonaldo et al. [10,11] provide a projection of the wave climate expected in the Adriatic Sea in the period 2071–2100 under an RCP 8.5 scenario. Their results suggested that, over the long term, a generalized decrease in longshore sediment drift can be envisaged along most of the Italian coast.

As pointed out by Ranasinghe [12], while calculating hydrodynamics on a grid produces robust and stable results, this is not straightforward for morphodynamics, since errors and instabilities frequently arise. For instance, Casas-Prat et al. [13] evaluated the impact on the coastal sediment transport along the Catalan coast (NW Mediterranean Sea) derived from climate projections and highlight the rise in climate model bias especially for longshore sediment transport, for which wave direction plays an important role. Therefore, Ranasinghe [12] suggested that a solution could be to develop and adopt an aggregated hydrodynamic forcing to simulate morphological change.

Several representative parameters can be used to estimate the variations in terms of wave climate, for instance, the evaluation of the mean significant wave heights, the percentile or the waves associated with specific return periods, whereas, in order to quantify the sediment dynamics modification, a wave morphologically equivalent to the complete wave regime (H_{ME}) can be evaluated. This representative wave, widely considered in the literature, can be used instead of wave time series to reduce computational time in morphological models (Chonwattana et al. [14], Plecha et al. [15]) or to describe the dominant sediment transport processes at the selected site (Buccino et al. [16]).

The present study further investigates the climate change effect and in particular focuses the analysis on the variation in terms of sediment transport, taking advantage of the H_{ME} parameter. The three analyzed wave datasets along the Italian Adriatic coast were obtained by Benetazzo et al. [1], including one historic dataset (from 1981 to 2010) and two future scenarios (2021–2050) based on the Representative Concentration Pathway 4.5 (RCP 4.5) and 8.5 (RCP 8.5) proposed by the IPCC [17]. The paper is organized as follows. Section 2 briefly describes the investigated coast, the wave datasets and the chosen representative analysis (mean value, percentile, extreme wave and morphological equivalent wave). In the third section, the results are presented for the historic and future runs and comparisons are performed to highlight the main findings. Finally, conclusions are drawn.

2. Materials and Methods

2.1. Investigated Area

The Adriatic Sea is a narrow rectangular-shaped semi-enclosed basin (Figure 1), about 750 km long and 200 km wide, and is connected to the Mediterranean Sea at its southern end by the Strait of Otranto, which is about 80 km wide. Its depth is rather limited in the northern part, where the bottom descends south-eastwards with a 1 in 1000 slope.

The Italian Adriatic coast is almost 1200 km long and stretches between Trieste at the north end and Capo d'Otranto at the south end. The coast is subdivided into 7 administrative regions: Friuli Venezia Giulia (FVG), Veneto (VEN), Emilia Romagna (ER), Marche (MAR), Abruzzo (ABR), Molise (MOL) and Puglia (PUG). This littoral zone is characterized by low sandy or gravel beaches and rocky cliffs, and there are also some large lagoon systems in the northern part. Several touristic activities and commercial and public fishing ports lay in this coastal area, being very important for the Italian economy.

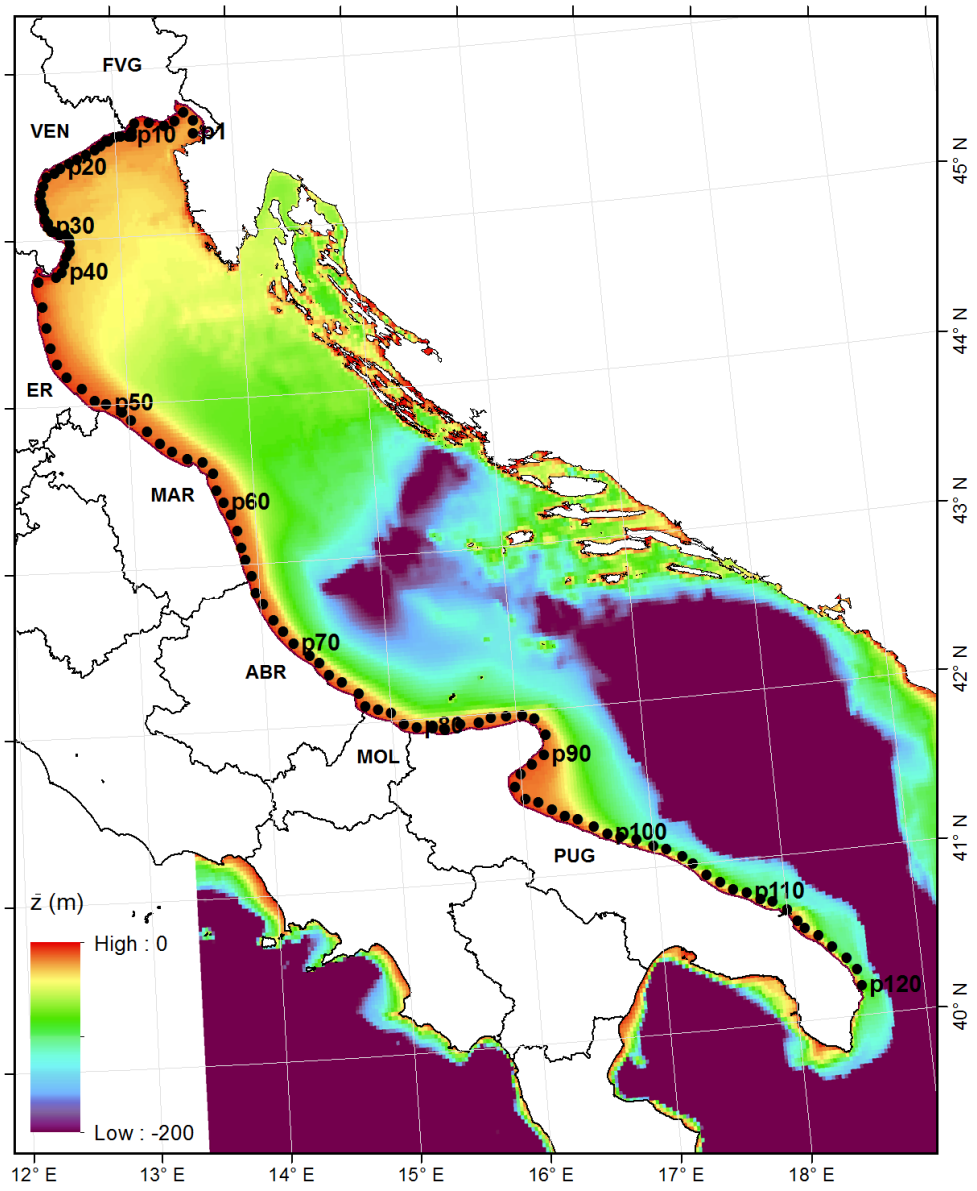

Figure 1. Wave model bathymetry in the Adriatic Sea and locations of the 120 points along the Italian Adriatic coast where the wave characteristics are extracted. The boundaries of the Italian administrative regions are highlighted with the abbreviations of the 7 that face the Adriatic Sea.

More in detail, the Friuli Venezia Giulia coast is characterized by rocky sea cliffs from the border with Slovenia to the mouth of the Timavo River and by low sandy beaches in the remaining part. This coastal zone also includes two large lagoon systems (named Marano and Grado lagoons) between the Isonzo and Tagliamento Rivers. Along this littoral, some important cities lay, such as Trieste, Muggia and Monfalcone, with their respective industrial and port areas, and two important tourist centers, Grado and Lignano.

The Venetian coastline is 160 km long and bordered by the Tagliamento River mouth at the north end and the Po di Goro River mouth at the south end (Ruol et al. [18]). This area is characterized by low beaches, three lagoon systems (Caorle, Venice and Po River Delta) and seven river mouths. In the northern part, with several important touristic cities (such as Carole, Eraclea, Jesolo, Venice, Rosolina), the coast is protected against erosion by many coastal structures. The southern part comprises the Po River Delta, the largest Italian wetlands with high environmental importance where the coast is characterized by a

sequence of low sandy and vulnerable barrier islands that separate lagoons and fishing valleys from the sea.

The Emilia-Romagna coast is 130 km long and stretches between the wetlands of Po River Delta and the area of Cattolica (Capolupo et al. [19]). It is formed by low sandy beaches that face erosion problems and high subsidence rates. Almost 50% of Emilia Romagna's coast is protected by coastal structures, parallel or perpendicular to the shore. It is a highly urbanized littoral zone with many touristic centers (Marina di Ravenna, Cesenatico, Rimini, Riccione, etc.).

The Marche coastline is about 180 km long and is bounded by the promontory of Gabicce Mare at the north end and by the Tronto River mouth at the south end. The littoral is relatively flat and straight and formed by sandy or gravel beaches, except for the hilly area between Gabicce and Pesaro and the eastern slopes of Monte Conero near Ancona. Some relevant touristic cities lay on this zone, such as Fano, Pesaro, Ancona, Sirolo, Numana and Porto Recanati.

The Abruzzo coastline has a total length of about 130 km (Pasquali and Marucci [20]). It is a heterogeneous coast characterized by low and sandy beaches and high and rocky stretches. There are productive and touristic activities that have recently encouraged an increase in human activity in the proximity of the Giulianova harbor and the city of Pescara. In the southern part, there is a massive presence of agricultural activities not far from the coast.

The Molise coast is approximately 36 km long and bounded to the north and south by the mouths of the Formale del Molino channel and the Saccione Stream (Minervino Amodio et al. [21]). In the 13 km long central portion, the coast is characterized by sea cliffs, and in the other parts the coast is low and sandy. Several touristic facilities and three harbor structures are present along the Molise coast.

Finally, the Adriatic Apulian coastline extends over about 450 km and is characterized by sandy and rocky beaches, coastal cliffs and stretches of mixed sediments, including pebbly beaches (Capolupo et al. [19], Bruno et al. [22]). As of recently, the Apulia region enjoys growing interest both from the national and the international tourism markets.

Two prevailing winds blow along the Adriatic Sea: the Sirocco wind that blows from the southeast as a basin response to large-scale weather events in the Mediterranean Sea, and the Bora wind from the northeast, driven by the complex orography of the Dinaric Alps on the east of the Adriatic. Both types of winds generate energetic sea states, i.e., large waves and high storm surges that plague the Adriatic coast, causing coastal erosion and marine flooding.

Recently, two extreme events occurred along the Adriatic Sea in October 2018 and in November 2019. On 29 October 2018, a very severe storm affected the Adriatic Sea as a consequence of explosive cyclogenesis in the Western Mediterranean Sea (Cavaleri et al. [23]). The intense winds from the southeast generated extreme waves (up to 6 m) and high water levels. On 12 November 2019, a severe storm event occurred, and the water level reached 1.82 m ZMPS at 22.50 UTC in the Northern Adriatic Sea, the second-highest value ever measured in this area. The combination of an astronomical tidal peak, a severe storm surge generated by a strong wind (up to 30 m/s) and a sudden pressure drop down to 987 hPa caused such a high level (Cavaleri et al. [24]). During these events, several failures occurred along the Adriatic coast and in particular in the Venetian littoral, which was affected by localized erosions and even by coastal flooding phenomena that caused damage to many touristic and productive facilities.

2.2. Wave Modeling in the Adriatic Sea

The wave dataset along the Italian Adriatic coast was obtained by Benetazzo et al. [1], forcing a spectral wave model with corrected ERA5 atmospheric wind fields. The correction was implemented to simulate the historical and future climate at a basin-scale (the Adriatic Sea). For this purpose, ERA5 winds were adjusted to match (in a statistical sense) those produced by high-resolution Regional Climate Models (RCM).

The details of the methodology used in the cited paper are briefly summarized below. The original ERA5 dataset includes global, hourly estimates of atmospheric variables at a native lon/lat resolution of 0.28125° and 137 vertical levels from the surface to 0.01 hPa. For storage purposes, data were gridded to a regular lat/lon grid of 0.25° and only the horizontal wind speed U_{10} were considered for the 30 years spanning from 1981 to 2010 over a region that encloses the Adriatic Sea and a large portion of the Mediterranean Sea surrounding the Italian peninsula.

The RCM wind fields in the Adriatic Sea were produced with the COSMO-CLM model (CCLM; Rockel et al. [25]). The wind field comprises the zonal and meridional components of U_{10}, available with a daily temporal resolution. The data span the Italian peninsula and a large portion of the surrounding Mediterranean Sea (lon range: 2° E–22.3° E; lat range: 35.7° N–47.6° N), with a spatial resolution of 0.0715° (approximately 8 km). The CCLM was run with the following three forcing setups, thus creating three corresponding datasets:

(i) Historical run (HR), from 1981 to 2010;
(ii) Future intermediate scenario Representative Concentration Pathway 4.5 run (RCP 4.5) from 2021 to 2050;
(iii) Future worst-case scenario RCP 8.5 run (RCP 8.5) from 2021 to 2050.

The reason why these two scenarios were chosen is that RCP 8.5 is considered to represent a "business as usual" scenario and the RCP 4.5 scenario is investigated as a more likely condition. The analysis of the other scenarios considered in the IPCC report is not particularly informative since the RCP 6.0 is very similar to the 4.5 one and the RCP 2.6 appears desirable but too optimistic. In addition, the new IPCC AR6 report (2021, [26]) recently identified high-emission scenarios (e.g., SSP5–8.5) with low likelihood and mid-range scenarios (e.g., SSP2–4.5) as more likely. Of course, all scenarios are not competing forecasts but rather tools to assess risk (Schwalm et al. [27]).

The quantile–quantile matching method (Wood et al. [28]) was used to bias-correct the systematic errors of ERA5 data using the RCM data as a reference. The result is RCM-adjusted ERA5 hourly wind fields for the present-day period (years 1981–2010) and the two near-future period (years 2021–2050) relative to RCP 4.5 and RCP 8.5. For simplicity, the input wind dataset for the HR, RCP 4.5 and RCP 8.5 does not include changes with regard to the wind direction, since the RCM wind field directions showed insignificant differences. Consequently, it is expected that the changes in terms of wave direction among the different scenarios are minor and only depend on the wave propagation processes. The simplification is acceptable also in view of the findings of Denamiel et al. [4]. Using a pseudo-global warming method, changing temperature, humidity and horizontal wind velocities, they found that the wave direction for extreme Sirocco events were totally unchanged between historic and future scenarios. A few differences were only found relative to specific events characterized by Bora winds in the North Adriatic Sea, for which future scenarios predicted a shift of the position of the interface separating waves propagating from very different directions.

The wave simulations in the Adriatic Sea have been carried out with the latest version 6.07 of the state-of-the-art spectral wave model WAVEWATCH III® (WW3, version 6.07, creator NOAA/NWS/NCEO/MMAB, College Park, MD, USA, Tolman [29]). WW3 solves the random phase spectral action density balance equation for wavenumber–direction spectra. For the future climate runs, the water level was uniformly raised by 0.12 m, by extrapolating, without distinction between RCPs, the present observed rate of the rise in the Mediterranean Sea level (2.8 mm/year; MedECC [30]) to the 2021–2050 period (to consider the sea level rise between the historic and future simulations). The grid used is regular with 361 × 280 nodes and rectangular cells of 0.025°. The model bathymetry (Figure 1) was obtained by interpolating a high-resolution bathymetric dataset of 0.0625′ (https://www.emodnet-bathymetry.eu, accessed on 15 July 2022) on the grid. The frequency grid is subdivided into 32 bins, ranging between 0.07 and 1.34 Hz. Frequencies are geometrically distributed with a ratio of 1.1 between one frequency and the next. The directions are uniformly distributed between 5° and 355°, with an interval of 10°. For the stability of the

numerical method adopted, the time discretization (four timesteps in WW3) is determined automatically from the physical grid characteristics. In particular, the following timesteps Δt were used: Δt (global) = 600 s; Δt (x, y) = 150 s; Δt (k, ϑ) = 300 s; Δt_{min} = 10 s.

2.3. Average and Extreme Value and Morphological Analyses

This paragraph describes the three types of analysis applied to the three datasets of modeled wave heights, relative to the simulations covering the 30-year periods 1981–2010 and 2021–2050 (two IPCC scenarios 4.5 and 8.5).

The first analysis deals with the mean wave climate and involves the identification of mean values and percentiles in order to highlight possible seasonality trends and find if the storminess of the future dataset is higher or lower than the historic one. For this purpose, the 50th and 99th total and monthly percentiles of *Hs* are computed for each point along the coastline.

The second analysis is used to describe the extreme wave conditions and to assess the wave height associated with specified return periods (T_R). The extreme value analysis is achieved through the simple box maxima method that consists of dividing the observation period into non-overlapping periods of equal size and restricts attention to the maximum observation in each period (Ferreira and de Haan [31]). The chosen sample is the yearly maxima that allows obtaining consistent and comparable statistics for all the grid points and scenarios, because the number of extremes in the sample is fixed. The Gumbel [32] distribution function is suitable to describe the extreme value distribution of this sample of independent, identically distributed (i.i.d.) values. The cumulative probability expression of this function is (Equation (1)):

$$P(x) = \exp\left[-\exp\left(\frac{x-\alpha}{\varphi}\right)\right] \quad (1)$$

where α is the location parameter and φ is the scale parameter. The selection of the *pdf* parameters is based on the Maximum Likelihood procedure.

The third analysis deals with the assessment of the longshore sediment transport patterns along the coast through the concept that we may define as morphologically equivalent wave (H_{ME}). The H_{ME} evaluation is based on the equivalence between the longshore sediment transport caused by the actual wave climate and by a single representative wave. The longshore sediment transport formula used to force this requirement is the well-known CERC formula [33]. The equivalence is based on the following condition (Equation (2)):

$$H_{ME}{}^{5/2} \sin(2\alpha_{ME})\, f_{ME} = \sum_i H_i{}^{5/2} \sin(2\alpha_i)\, f_i \quad (2)$$

where H_i is all the simulated significant wave heights, α_i is the corresponding wave obliquities and f_i is their frequency of occurrence, equal to $1/N$ (N = number of simulated sea states). The calculation of H_{ME} is performed for each dataset by subdividing the waves based on the sign of the wave obliquity, i.e., generating sediment transport directed towards opposite directions (e.g., north and south). In addition, f_{ME} is the frequency of the total number of waves coming from one of the two directions, and the wave obliquity α_{ME} is (arbitrarily) taken a priori equal to $\pm\pi\pi/4$. The waves are also subdivided into three classes based on their height: (i) *Hs* > 0.5 m; (ii) *Hs* < 2 m; (iii) *Hs* > 2 m. The first class is used to estimate the general longshore sediment transport. The second class influences only the sediment transport that occurs close to the shoreline. The sediment transport that occurs in a region not so close to the shoreline, potentially offshore of the coastal structures (groins and detached breakwaters), is only affected by the sediment transport computed for the third class.

In an area without structure the reference wave climate is the result of class (i). In the presence of structures, and in particular an array of groins, we can distinguish between the movements of the sediments confined by the groins, which have only a local effect (the results of class (ii) only affect these movements), and the movements occurring outside

the groins as roundhead, which influences the morphological response at large scale. This latter response is affected only by the results of class (iii).

3. Results

The wave characteristics are extracted from 120 points (or virtual wave buoys) along the Italian Adriatic coast, approximately 5 km from the shoreline. The list of locations is shown in Figure 1 and reported in Table 1. The points are named from 1 to 120 starting from the northern side and are placed in front of the seven Italian administrative regions. The table proposes a reference list of points that may form a baseline for future comparisons.

Table 1. Name, locations, depth and corresponding administrative Italian region of the 120 points (or virtual wave buoys) along the Adriatic coast where the wave characteristics are extracted.

Name	Lon (°)	Lat (°)	z (m)	Region	Name	Lon (°)	Lat (°)	z (m)	Region	Name	Lon (°)	Lat (°)	z (m)	Region
p1	13.675	45.6	−23	FVG	p41	12.45	44.775	−15	VEN	p81	15.325	41.95	−19	PUG
p2	13.675	45.675	−22	FVG	p42	12.3	44.75	−8	ER	p82	15.425	41.925	−13	PUG
p3	13.6	45.725	−13	FVG	p43	12.325	44.6	−11	ER	p83	15.55	41.95	−17	PUG
p4	13.525	45.675	−11	FVG	p44	12.35	44.475	−12	ER	p84	15.7	41.95	−14	PUG
p5	13.425	45.65	−10	FVG	p45	12.375	44.35	−10	ER	p85	15.8	41.975	−18	PUG
p6	13.3	45.675	−9	FVG	p46	12.425	44.25	−9	ER	p86	15.925	41.975	−18	PUG
p7	13.175	45.675	−8	FVG	p47	12.5	44.175	−10	ER	p87	16.05	41.975	−22	PUG
p8	13.15	45.625	−14	FVG	p48	12.625	44.1	−11	ER	p88	16.15	41.95	−21	PUG
p9	13.15	45.6	−16	VEN	p49	12.725	44.025	−11	ER	p89	16.225	41.85	−16	PUG
p10	13.125	45.6	−17	VEN	p50	12.825	44	−13	MAR	p90	16.2	41.725	−14	PUG
p11	13.05	45.6	−14	VEN	p51	12.95	43.95	−14	MAR	p91	16.1	41.675	−12	PUG
p12	13	45.6	−12	VEN	p52	13.025	43.9	−14	MAR	p92	16	41.625	−11	PUG
p13	12.95	45.575	−14	VEN	p53	13.15	43.825	−14	MAR	p93	15.95	41.55	−11	PUG
p14	12.925	45.575	−12	VEN	p54	13.25	43.75	−13	MAR	p94	16.025	41.475	−14	PUG
p15	12.875	45.55	−15	VEN	p55	13.35	43.7	−14	MAR	p95	16.125	41.45	−16	PUG
p16	12.825	45.525	−16	VEN	p56	13.475	43.65	−15	MAR	p96	16.225	41.4	−18	PUG
p17	12.75	45.5	−15	VEN	p57	13.6	43.625	−17	MAR	p97	16.325	41.35	−17	PUG
p18	12.675	45.475	−16	VEN	p58	13.675	43.55	−16	MAR	p98	16.425	41.325	−21	PUG
p19	12.6	45.45	−16	VEN	p59	13.7	43.45	−12	MAR	p99	16.55	41.275	−36	PUG
p20	12.525	45.425	−16	VEN	p60	13.75	43.375	−13	MAR	p100	16.65	41.225	−37	PUG
p21	12.475	45.4	−15	VEN	p61	13.8	43.3	−14	MAR	p101	16.75	41.2	−50	PUG
p22	12.4	45.375	−11	VEN	p62	13.85	43.2	−14	MAR	p102	16.875	41.175	−70	PUG
p23	12.375	45.325	−14	VEN	p63	13.875	43.1	−13	MAR	p103	17	41.125	−59	PUG
p24	12.35	45.275	−16	VEN	p64	13.9	43.025	−13	MAR	p104	17.1	41.1	−60	PUG
p25	12.35	45.225	−17	VEN	p65	13.95	42.925	−13	MAR	p105	17.225	41.05	−71	PUG
p26	12.35	45.2	−15	VEN	p66	13.975	42.825	−12	ABR	p106	17.3	41	−72	PUG
p27	12.375	45.175	−17	VEN	p67	14.025	42.75	−13	ABR	p107	17.4	40.925	−38	PUG
p28	12.375	45.125	−15	VEN	p68	14.1	42.65	−15	ABR	p108	17.5	40.875	−43	PUG
p29	12.4	45.1	−19	VEN	p69	14.175	42.575	−17	ABR	p109	17.6	40.825	−49	PUG
p30	12.4	45.075	−14	VEN	p70	14.25	42.5	−17	ABR	p110	17.7	40.8	−66	PUG
p31	12.425	45.05	−9	VEN	p71	14.375	42.425	−21	ABR	p111	17.8	40.75	−61	PUG
p32	12.45	45.05	−16	VEN	p72	14.45	42.375	−21	ABR	p112	17.9	40.725	−83	PUG
p33	12.5	45.025	−19	VEN	p73	14.525	42.3	−16	ABR	p113	18	40.675	−60	PUG
p34	12.55	45.025	−29	VEN	p74	14.625	42.25	−20	ABR	p114	18.075	40.6	−22	PUG
p35	12.575	45	−28	VEN	p75	14.75	42.175	−19	ABR	p115	18.125	40.55	−27	PUG
p36	12.575	44.975	−17	VEN	p76	14.8	42.1	−12	ABR	p116	18.225	40.5	−37	PUG
p37	12.575	44.925	−15	VEN	p77	14.9	42.075	−18	MOL	p117	18.325	40.425	−73	PUG
p38	12.55	44.9	−14	VEN	p78	15	42.05	−23	MOL	p118	18.425	40.35	−97	PUG
p39	12.525	44.85	−17	VEN	p79	15.1	41.975	−16	MOL	p119	18.5	40.275	−98	PUG
p40	12.5	44.8	−19	VEN	p80	15.2	41.95	−16	PUG	p120	18.525	40.175	−67	PUG

Figure 2 shows the wave roses in 11 of these locations along the Italian Adriatic coast relative to the historical run (1981–2010) highlighting the main wave direction along the coast. All the plotted wave climates are bimodal since they are influenced by the two prevailing wind regimes, Bora and Scirocco.

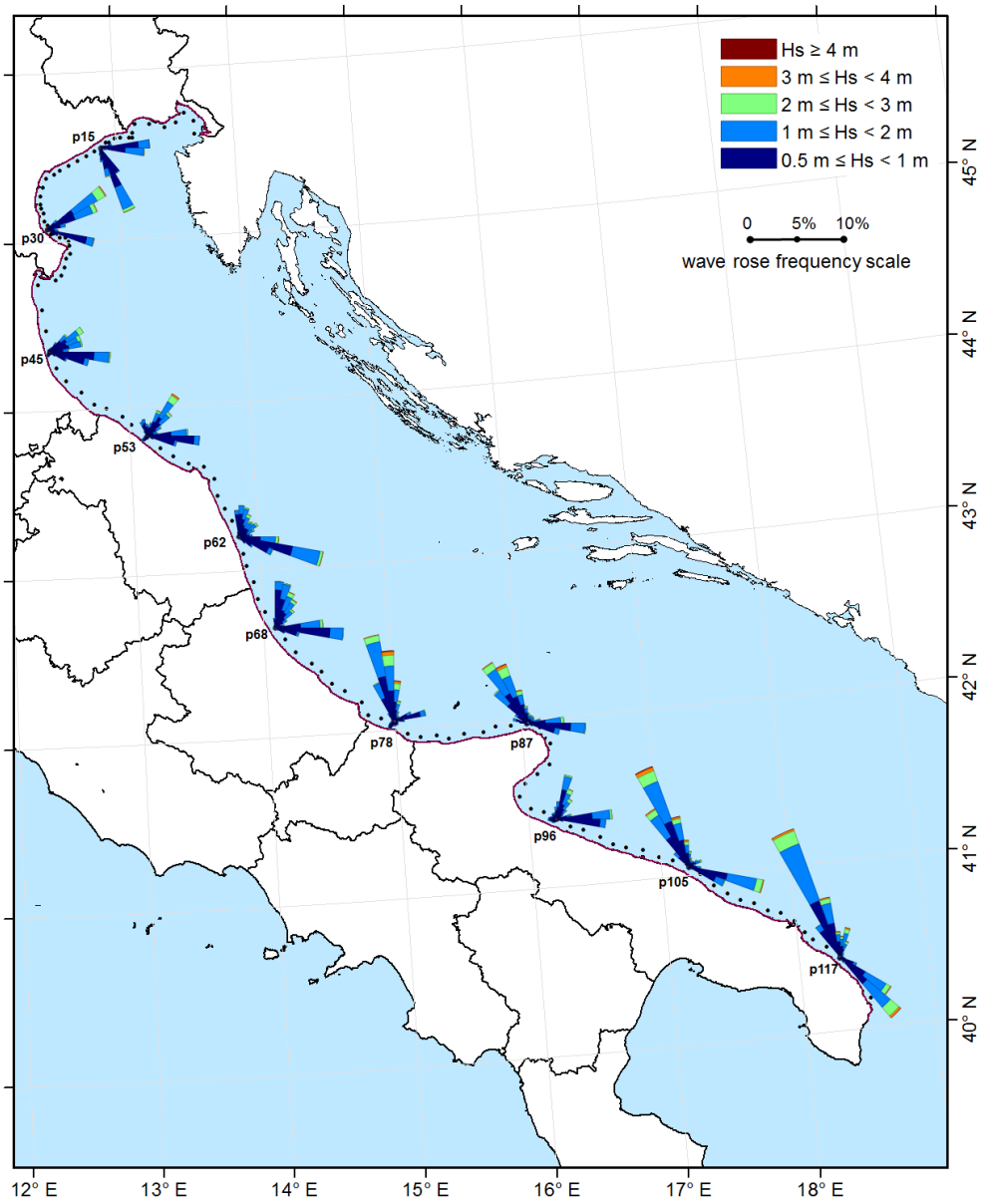

Figure 2. Wave roses in some of the 120 virtual wave buoys along the Adriatic coast of Italy relative to the historical run (1981–2010) highlighting the main wave direction along the coast.

The following Section 3.1. presents, in all 120 points, the results of the average and extreme value analyses, comparing the historic and future scenarios. Section 3.2. describes the results of the morphological analysis for the historic run and Section 3.3. compares the results of the morphological analyses relative to the historic and future scenarios.

3.1. Comparison between Historical and Future Average and Extreme Value Analyses

The computed time series of significant wave heights are analyzed in terms of mean wave climate. In general, the highest waves are estimated in the deep Southern Adriatic Sea and the mildest climate is in the shallow and protected Gulf of Trieste. Both future scenarios produce a decrease in the significant wave height *Hs*. In short, the total averaged reduction

between the historic run and the RCP 4.5 scenario is in the range of 2–7%, with the higher reductions between points 30 and 53. For the RCP 8.5 scenario, the decrease is in the range of 0–8% with the highest reductions between points 28 and 33 and almost no reduction in the southern area. In terms of wave period and wave direction, no significant variations are observed between the historic and future scenarios. A slightly northward rotation of 5° of wave direction is predicted for points between 47 and 78. The relation between the significant wave height and the peak wave period can be described by $Tp = a\,Hs^b$. On average, the a coefficient is 5.53 and the b coefficient is 0.34.

Figures 3 and 4 show the comparisons between the 50th and 99th percentiles of the significant wave heights *Hs* computed at the 120 virtual buoys along the Italian Adriatic coast relative to the historic run (HR) and future scenario runs, respectively (RCP 4.5 and RCP 8.5 scenarios). The 50th percentile is not substantially affected by climate change effects and the average reduction is only of the order of 1–2%, whereas the 99th percentile is subject to a larger average reduction. Data can be divided into two groups: (i) points from 5 to 56 (blue–light blue points in the figures), located in the Northern Adriatic stretch, are affected by reductions of 6% for the RCP 4.5 scenario and 9.5% for the RCP 8.5 scenario; (ii) the remaining points (orange–red) are affected by reductions of the order of 4% for the intermediate scenario and of 5.5% for the worst-case scenario. The few virtual buoys of group (ii) that appear mixed with group (i) are number 91–94, located in the area sheltered by the Gargano peninsula.

These data predict, especially for the upper stretch of the Italian Adriatic coast, a small reduction in the wave storminess of the future scenario compared to the historical one, even if the mean sea level is higher (and thus potentially inducing larger waves).

Figure 5 shows the change for the largest wave conditions based on the extreme value analysis, which identifies independent storms, rather than the 99th percentile evaluation shown in Figure 4. The analysis confirms the previous observation. The figure compares the historic and future runs in terms of 30-year return period significant wave heights *Hs* computed at the 120 virtual buoys. The average reduction for the intermediate scenario is about 3% and for the worst-case scenario is about 5%. In addition, for these comparisons, some locations show a different decrease trend: the 30 y *Hs* values for virtual buoys 19–41 are 6.5% and 10% smaller than the historic run for the RCP 4.5 and RCP 8.5, respectively.

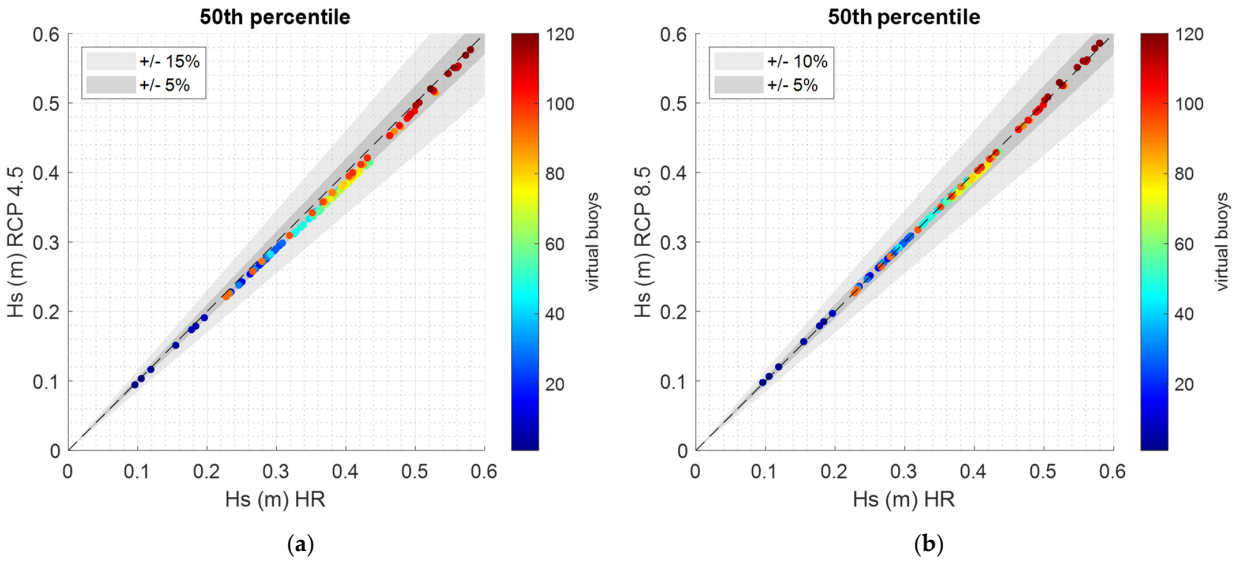

Figure 3. Comparison between the 50th percentiles of the significant wave heights *Hs* computed at the 120 virtual buoys along the Italian Adriatic coast relative to the historic run (HR) and future scenario runs: (**a**) historic run vs. RCP 4.5 scenario; (**b**) historic run vs. RCP 8.5 scenario.

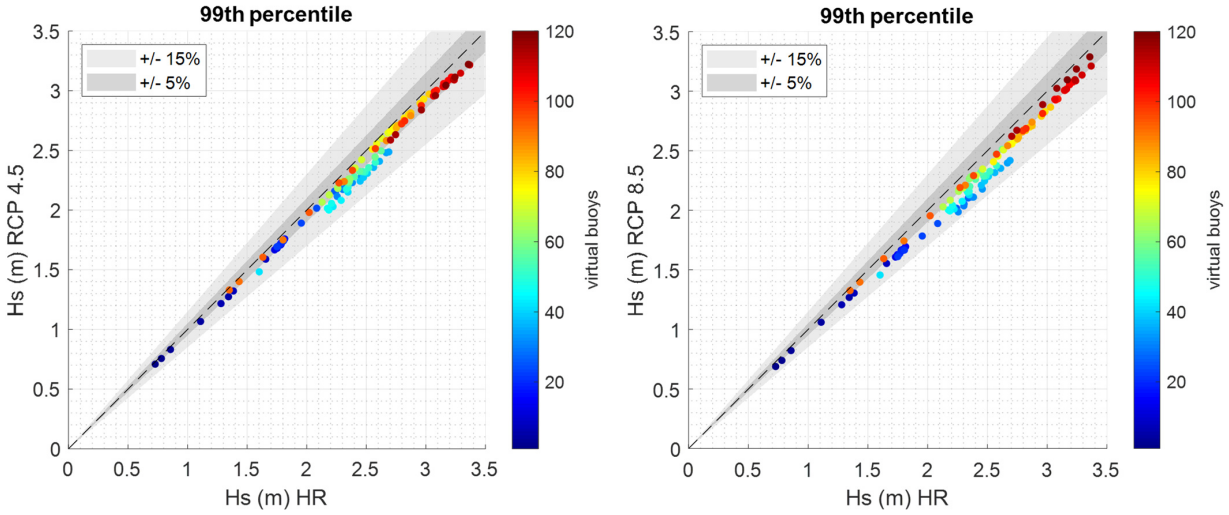

Figure 4. Comparison between the 99th percentiles of the significant wave heights *Hs* computed at the 120 virtual buoys along the Italian Adriatic coast relative to the historic run (HR) and future scenario runs: (**a**) historic run vs. RCP 4.5 scenario; (**b**) historic run vs. RCP 8.5 scenario.

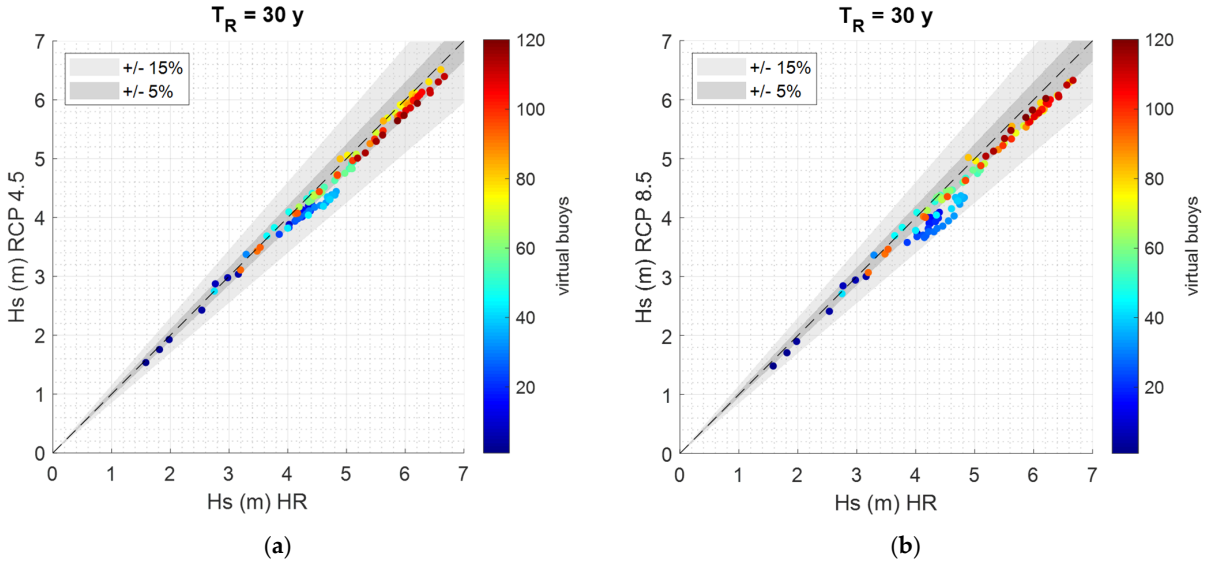

Figure 5. Comparison between the 30-year return period significant wave heights *Hs* computed at the 120 virtual buoys along the Italian Adriatic coast relative to the historic run (HR) and future scenario runs: (**a**) historic run vs. RCP 4.5 scenario; (**b**) historic run vs. RCP 8.5 scenario.

Figure 6 shows the monthly trends of the 99th percentiles for all the points. Higher waves are correctly predicted for the winter season (from October to March, [34]), and the trend remains unchanged for the future scenario with a decrease in terms of *Hs* magnitude as argued above. The color code is the same used in the previous figures. The blue/light blue points relative to the upper Adriatic coast show a marked difference between autumn and spring, with a peak in November which is consistent with the timing of the highest storms that occurred in this area (1966, 2018, 2019, Canestrelli et al. [35], Cavaleri et al. [23,24]).

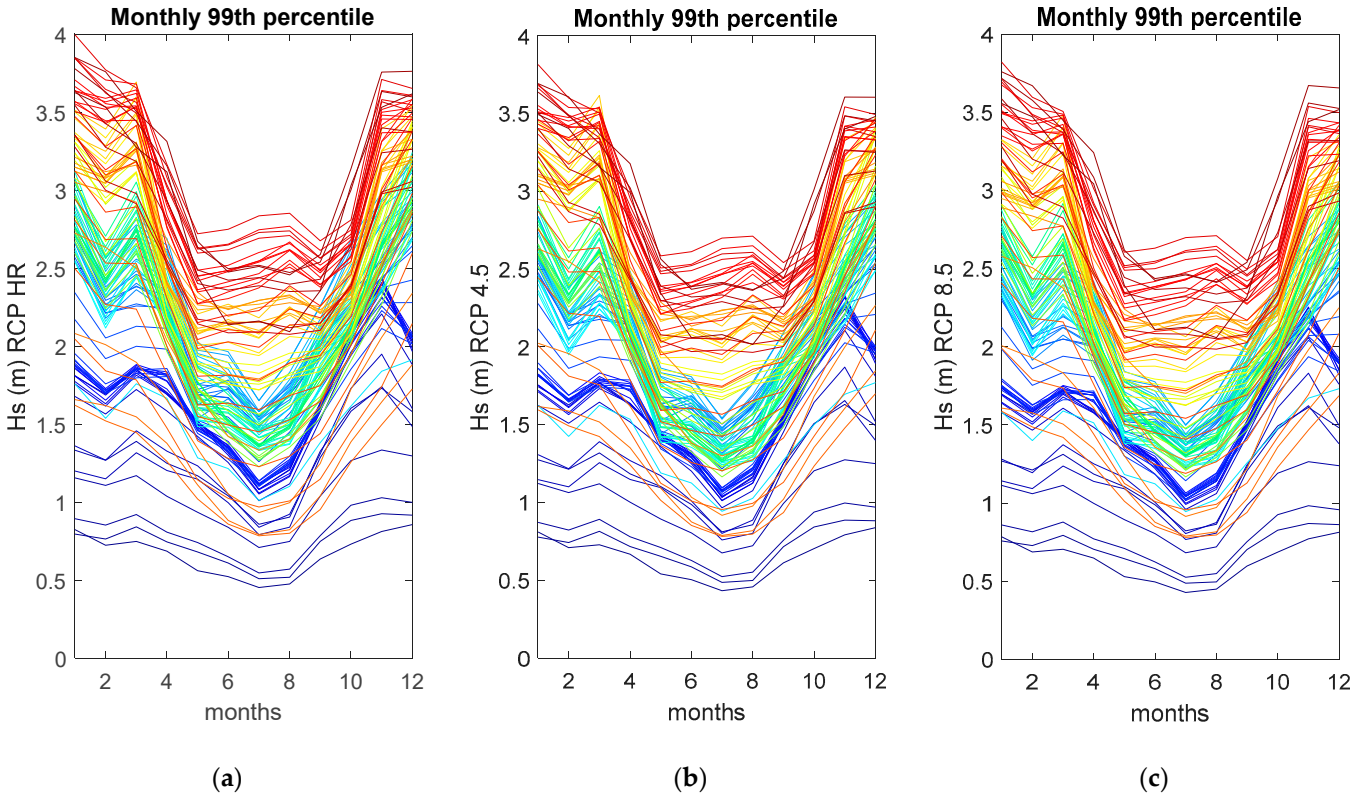

Figure 6. Monthly 99th percentiles of the significant wave heights *Hs* computed at the 120 virtual buoys along the Italian Adriatic coast (colors are the same used in the previous figures): (**a**) historic run (HR); (**b**) RCP 4.5 scenario; (**c**) RCP 8.5 scenario.

3.2. Morphological Equivalent Waves for the Historic Run

The morphological equivalent wave H_{ME} is computed by subdividing the waves based on their wave obliquity (positive and negative) to highlight the sediment transport directions and classifying their *Hs* into three classes: (i) *Hs* > 0.5 m, representative of the whole wave climate; (ii) *Hs* < 2 m, influencing the region close to the shore; and (iii) *Hs* > 2 m, important because the region far from the shore is the only one affected by these waves.

Figures 7 and 8 show the north (positive) and south directed (negative) values of H_{ME} computed for the first class. The figures also show the monthly values of H_{ME} and, as expected, the higher values are predicted during the winter season, or more precisely from October to March.

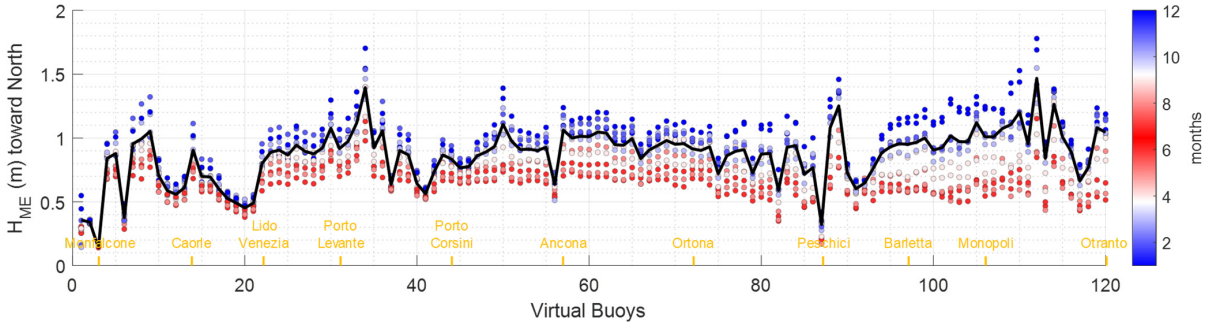

Figure 7. H_{ME} (black line) directed toward north, computed at the 120 virtual buoys along the Italian Adriatic coast relative to the historic run (HR). Colored dots are the monthly H_{ME} at the 120 locations and some locations are highlighted to increase the figure readability.

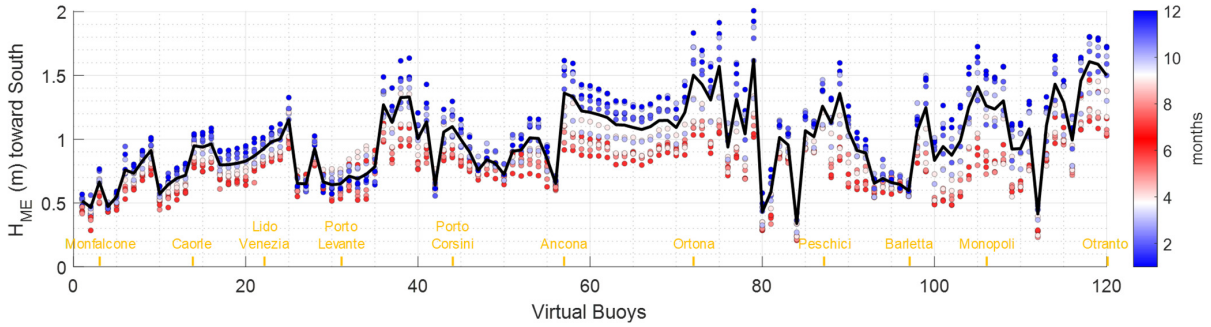

Figure 8. H_{ME} (black line) directed toward south, computed at the 120 virtual buoys along the Italian Adriatic coast relative to the historic run (HR). Colored dots are the monthly H_{ME} at the 120 points and some locations are highlighted to increase the figure readability.

The direction of the sediment transport is obviously given by the higher value between the north and south H_{ME}. In Figure 9, the direction of the sediment transport (calculated for the first class) is shown for all the locations along the Italian Adriatic Sea relative to the historic run. The figure also highlights where the points of divergence (yellow crosses in the figure) for sediment transport are located. The model reasonably predicts divergence points in correspondence to some important river mouths or inlets: the Grado lagoon inlet, the Tagliamento River mouth (between Lignano Sabbiadoro and Bibione), the Adige River mouth (north of Rosolina Mare), the Po River Delta, the Idrovia Ferrara-Ravenna (Porto Garibaldi), the Foglia River mouth (Pesaro, north of Fano), the Esino River mouth (between Senigallia and Ancona), the Acquarotta channel (Marina di Lesina), the Varano Lake inlet (north of Peschici) and the ports of Barletta, Molfetta, Polignano a Mare, Torre Santa Sabina and Brindisi.

The magnitude of the longshore sediment transport is related to the difference between the H_{ME} directed toward the north and south. Figure 10 shows this magnitude at the 120 virtual buoys along the Italian Adriatic coast relative to the historic run. Positive arrows indicate sediment transport directed toward the north; conversely, negative arrows indicate sediment transport directed toward the south. Light blue arrows are the net H_{ME} computed with the waves larger than 2 m (class (iii)) and purple arrows are the ones computed with waves smaller than 2 m (class (ii)). This subdivision allows for identifying the locations where the direction changes considering larger or smaller waves. Black dots in the lower part of the figure highlight these conditions. In almost all the points where the direction changes the net H_{ME} is small (<0.4 m), except for the points in front of Lido di Venezia and Pellestrina, the two islands that separate the Venetian lagoon from the sea. These two stretches of coast are pocket beaches delimited by long breakwaters that protect the lagoon inlets. In both islands, the coast is protected by groins and therefore the large-scale morphological evolution is dominated by the net north-directed sediment transport relative to class (iii) ($Hs > 2$ m). The net south-directed sediment transport relative to class (ii) ($Hs < 2$ m) affects only the local morphological response occurring in the vicinity of the shoreline.

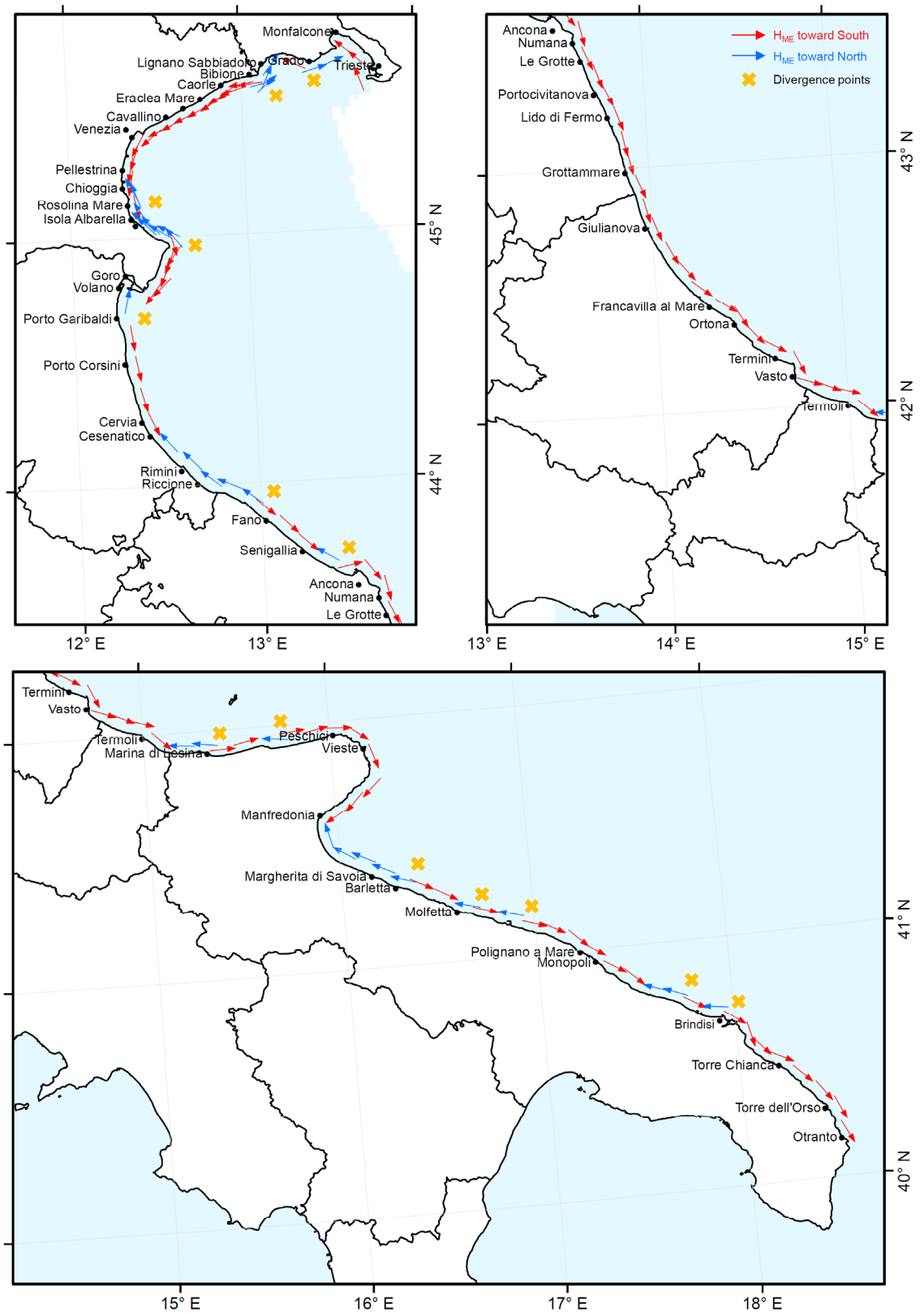

Figure 9. Direction of the morphological wave heights H_{ME} along the Italian Adriatic coast. The H_{ME} value is evaluated taking into account all waves with $Hs > 0.5$ m for the historic run.

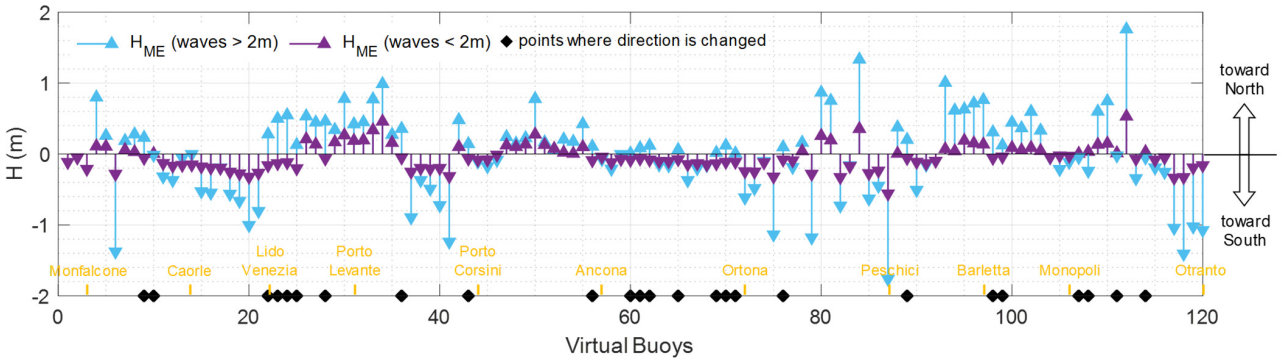

Figure 10. Magnitude of the net morphological equivalent waves H_{ME} at the 120 virtual buoys along the Italian Adriatic coast relative to the historic run (HR). Positive arrows indicate sediment transport directed toward north; conversely, negative arrows indicate sediment transport directed toward south. Light blue arrows are the H_{ME} computed with the waves larger than 2 m and purple arrows are the ones computed with waves smaller than 2 m.

3.3. Historic and Future Morphological Equivalent Waves

The net H_{ME} is also calculated for the two future scenarios and compared with the historic one. Figure 11 shows, in color scale, the ratio between the future and historic net H_{ME} taking into account all the waves larger than 0.5 m (class (i)). Figure 11a,b show the ratio for the RCP 4.5 and RCP 8.5 scenarios, respectively.

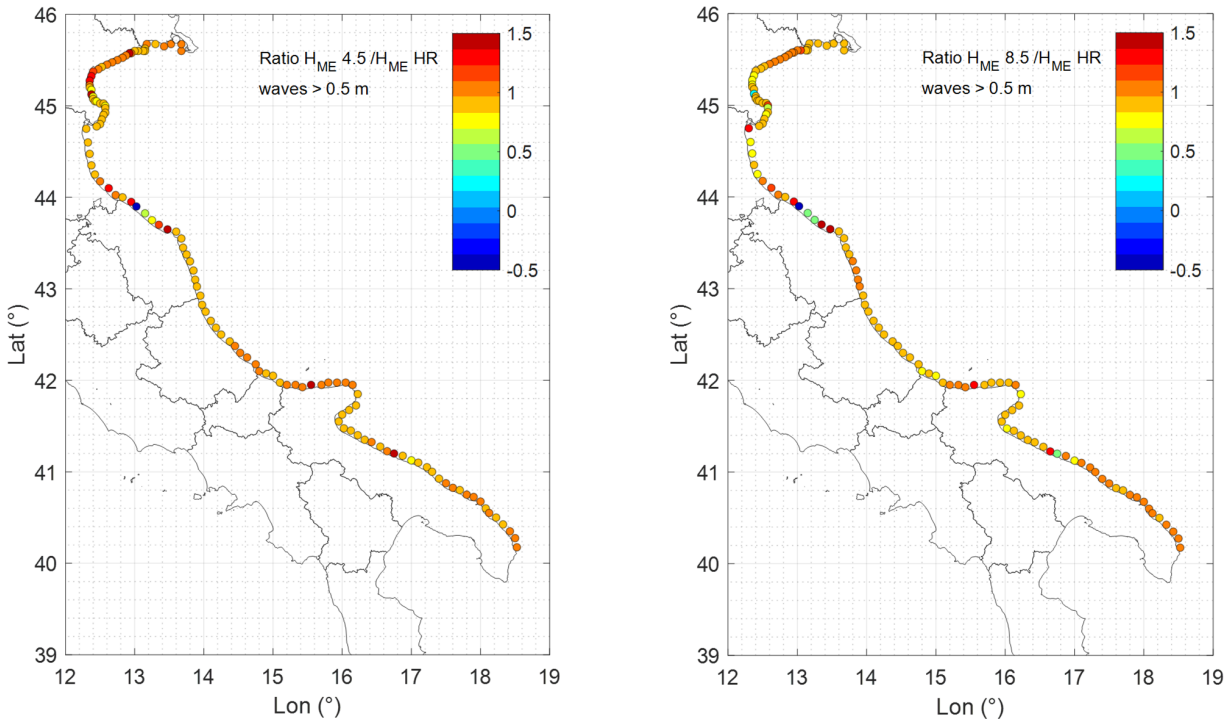

(**a**) (**b**)

Figure 11. Ratio between historic and future net H_{ME} computed with all the waves larger than 0.5 m at the 120 virtual buoys along the Italian Adriatic coast. (**a**) Historic run vs. RCP 4.5 scenario; (**b**) historic run vs. RCP 8.5 scenario. Blue points indicate that the direction of the sediment transport is changed.

For both future scenarios, even if the wave heights decrease on average, there are several areas where the net sediment transport increases, which is a consequence of the

different attenuation of north-directed and south-directed waves during the specific propagation pattern evaluated by the model in every grid point. For instance, in the Veneto region in front of Lido di Venezia, the ratio is larger than the one for the RCP 4.5 scenario.

Since south-directed net sediment transport is associated with negative H_{ME} values, a negative ratio is found where the direction of the sediment transport between the historic and future runs changes. This occurs only in one location close to Fano, where a blue point appears and where the climate change has therefore the largest effect in terms of net sediment transport from a qualitative (and quantitative) point of view.

The higher future scenario (RCP 8.5), associated with a milder climate as seen in Section 3.1, when divided by the historic condition gives smaller ratios, as expected. For instance, in front of Lido di Venezia the ratio is smaller than one.

Figure 12 shows the same comparisons calculating the net H_{ME} with all the waves larger than 2 m (class (iii)). This figure, which is important to investigate the sediment transport that occurs in a region not so close to the shoreline, potentially offshore of the coastal structures (groins and detached breakwaters), shows slightly different information. For instance, in the Emilia Romagna region, in front of the low-crested barriers of Punta Marina and Lido di Dante, the attenuation is more significant than for class (i) (orange–yellow in Figure 11, cyan in Figure 12). The practical consequence of this observation is an expected reduced erosion for these littorals.

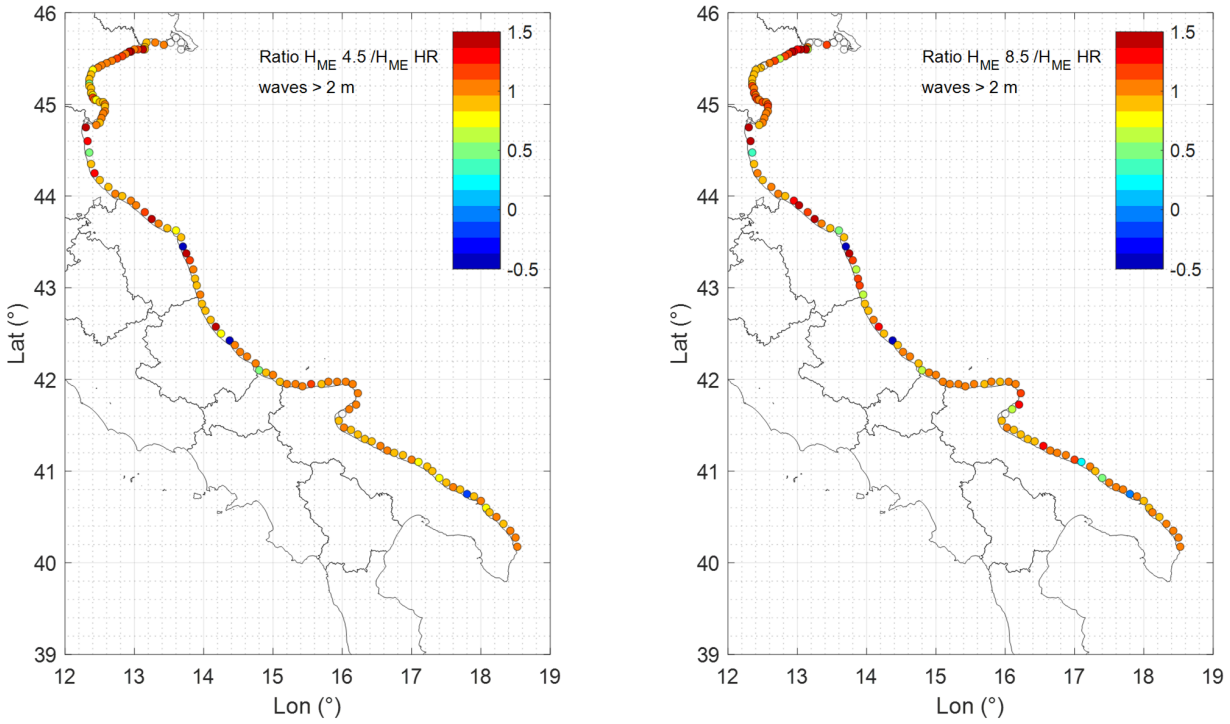

Figure 12. Ratio between historic and future net H_{ME} computed with all the waves larger than 2 m at the 120 virtual buoys along the Italian Adriatic coast. (**a**) Historic run vs. RCP 4.5 scenario; (**b**) historic run vs. RCP 8.5 scenario. Blue points indicate that the direction of the sediment transport is changed.

These figures give practical information to the coastal authorities for the management of the whole Adriatic shoreline. Further research is necessary to sufficiently incorporate the uncertainties associated with climate-change-driven coastal erosion modeling (Toimil et al. [36]), such as considering different emission scenarios, reducing model uncertainties and developing better datasets.

4. Conclusions

The paper analyzes the wave climate along the Adriatic Italian coast relative to a historic run (1981–2010) and two future scenarios (2021–2050) based on two IPCC Representative Concentration Pathways (4.5 and 8.5, [17]). The wave datasets are obtained with a spectral wave model forced with corrected ERA5 wind fields. The correction relies on a quantile–quantile matching method that modifies the reanalysis winds in order to match the local climate system relative to the investigated semi-enclosed basin. The time series are extracted in 120 virtual buoys located along the Adriatic coast, 5 km from the shoreline.

The first analysis deals with seasonality and quantiles of the wave climates. The observed seasonality trend is consistent with expectations, but it does not point out any effect of global change. The investigation identifies a reduction in the wave storminess. In particular, the comparison between the historic run and the future scenarios shows an overall reduction, especially in terms of the 99th percentile. The decrease is of the order of 3–6% for the RCP 4.5 scenario and 5–10% for the worst-case one, depending on the locations.

The observed storminess reduction close to the shore is not a trivial result. In fact, in relatively shallow waters (approximately 15 m), the sea level rise associated with the future scenario (0.12 m for both) is expected to induce slightly larger waves (see for instance the effect of water depth on the generated waves according to the formula by Hurdle and Stive [37]).

The second analysis describes the extreme wave height reduction, and in particular the wave heights associated with 30-year return periods. Even if the analyzed statistical sample is different from the one used to define the 99th percentile, the same reduction (3–6% and 5–10%) is found.

The conclusion of these two investigations is that, especially in the upper stretch of the Italian Adriatic coast, the expected increase in the coastal flooding hazard due to sea level rise is partially mitigated by a reduction in the (average and) extreme wave storminess.

The third analysis introduces the concept of morphologically equivalent wave (H_{ME}), a lumped value that represents the sediment transport. The concept is based on the equivalence between the longshore sediment transport computed using the CERC formula for the actual wave climate and for a lumped wave height value equal to H_{ME}. Positive and negative contributions are separated to point out their relative importance, and the net is obtained through the algebraic sum of the two contributions. Furthermore, the wave climate is subdivided in three classes: (i) $Hs > 0.5$ m; (ii) $Hs < 2$ m; (iii) $Hs > 2$ m. Therefore, three different (positive and negative) H_{ME} values are computed. The first class is used to estimate the general longshore sediment transport. The second class influences only the sediment transport that occurs close to the shoreline. The third is important to investigate the sediment transport that occurs in a region not so close to the shoreline, potentially offshore of the coastal structures.

For both future scenarios, even if the wave heights on average are smaller than the historic ones, the estimated net sediment transport for the first class is predicted to be larger in several areas (i.e., the Venetian littoral). This could be related to the different attenuation of north-directed and south-directed waves during the specific propagation pattern evaluated by the model in every grid point. For the third class, i.e., $Hs > 2$ m, a larger attenuation than for the first class, i.e., all waves, is found in some littorals (i.e., in some stretches of the Emilia Romagna coast). The practical consequence is a reduction in the transport in the offshore area which, where the coastline is protected by structures, is the most relevant area in terms of global coastal erosion. In general, the obtained results give for each location practical information to the coastal authorities for the actual and future management of the whole Adriatic shoreline.

Author Contributions: Conceptualization, P.R., L.M. and C.F.; methodology, L.M.; investigation, C.F.; resources, F.B.; writing—original draft preparation, C.F. and L.M.; writing—review and editing, C.F., L.M., F.B., A.B. and P.R.; supervision, P.R. and A.B. All authors have read and agreed to the published version of the manuscript.

Funding: This research was partially funded by the Venice 2021 research grant funded by Provveditorato for the Public Works of Veneto, Trentino Alto Adige and Friuli Venezia Giulia, provided through the concessionary of State Consorzio Venezia Nuova and coordinated by CORILA (Consorzio per il coordinamento delle ricerche inerenti al sistema lagunare di Venezia), and by the project "Development of a new Wave Energy Converter named Wave Attenuator", Bando Centro Giorgio Levi Cases a tema vincolato, Prot. 8 del 20 January 2021 Fasc. 2021-III/13.1.

Conflicts of Interest: The authors declare no conflict of interest.

References

1. Benetazzo, A.; Davison, S.; Barbariol, F.; Mercogliano, P.; Favaretto, C.; Sclavo, M. Correction of ERA5 Wind for Regional Climate Projections of Sea Waves. *Water* **2022**, *14*, 1590. [CrossRef]
2. Benetazzo, A.; Fedele, F.; Carniel, S.; Ricchi, A.; Bucchignani, E.; Sclavo, M. Wave climate of the Adriatic Sea: A future scenario simulation. *Nat. Hazards Earth Syst. Sci.* **2012**, *12*, 2065–2076. [CrossRef]
3. Intergovernmental Panel on Climate Change (IPCC). *Intergovernmental Panel on Climate Change: Fourth Assessment Report*; Intergovernmental Panel on Climate Change Secretariat: Geneva, Switzerland, 2007.
4. Denamiel, C.; Pranić, P.; Quentin, F.; Mihanović, H.; Vilibić, I. Pseudo-global warming projections of extreme wave storms in complex coastal regions: The case of the Adriatic Sea. *Clim. Dyn.* **2020**, *55*, 2483–2509. [CrossRef]
5. De Leo, F.; Besio, G.; Mentaschi, L. Trends and variability of ocean waves under RCP8. 5 emission scenario in the Mediterranean Sea. *Ocean Dyn.* **2021**, *71*, 97–117. [CrossRef]
6. Barbariol, F.; Davison, S.; Falcieri, F.M.; Ferretti, R.; Ricchi, A.; Sclavo, M.; Benetazzo, A. Wind Waves in the Mediterranean Sea: An ERA5 Reanalysis Wind-Based Climatology. *Front. Mar. Sci.* **2021**, *8*, 1–23. [CrossRef]
7. Caloiero, T.; Aristodemo, F. Trend Detection of Wave Parameters along the Italian Seas. *Water* **2021**, *13*, 1634. [CrossRef]
8. Caloiero, T.; Aristodemo, F.; Ferraro, D.A. Annual and seasonal trend detection of significant wave height, energy period and wave power in the Mediterranean Sea. *Ocean Eng.* **2022**, *243*, 110322. [CrossRef]
9. Grases, A.; Gracia, V.; García-León, M.; Lin-Ye, J.; Sierra, J.P. Coastal flooding and erosion under a changing climate: Implications at a low-lying coast (Ebro Delta). *Water* **2020**, *12*, 346. [CrossRef]
10. Bonaldo, D.; Bucchignani, E.; Pomaro, A.; Ricchi, A.; Sclavo, M.; Carniel, S. Wind waves in the Adriatic Sea under a severe climate change scenario and implications for the coasts. *Int. J. Climatol.* **2020**, *40*, 5389–5406. [CrossRef]
11. Bonaldo, D.; Antonioli, F.; Archetti, R.; Bezzi, A.; Correggiari, A.; Davolio, S.; De Falco, G.; Fantini, M.; Fontolan, G.; Furlani, S.; et al. Integrating multidisciplinary instruments for assessing coastal vulnerability to erosion and sea level rise: Lessons and challenges from the Adriatic Sea, Italy. *J. Coast. Conserv.* **2019**, *23*, 19–37. [CrossRef]
12. Ranasinghe, R. Assessing climate change impacts on open sandy coasts: A review. *Earth-Sci. Rev.* **2016**, *160*, 320–332. [CrossRef]
13. Casas-Prat, M.; McInnes, K.L.; Hemer, M.A.; Sierra, J.P. Future wave-driven coastal sediment transport along the Catalan coast (NW Mediterranean). *Reg. Environ. Chang.* **2016**, *16*, 1739–1750. [CrossRef]
14. Chonwattana, S.; Weesakul, S.; Vongvisessomjai, S. 3D Modeling of morphological changes using representative waves. *Coast. Eng. J.* **2005**, *47*, 205–229. [CrossRef]
15. Plecha, S.; Sancho, F.; Silva, P.; Dias, J.M. Representative waves for morphological simulations. *J. Coast. Res.* **2007**, *50*, 995–999.
16. Buccino, M.; Di Paola, G.; Ciccaglione, M.C.; Del Giudice, G.; Rosskopf, C.M. A medium-term study of Molise coast evolution based on the one-line equation and "equivalent wave" concept. *Water* **2020**, *12*, 2831. [CrossRef]
17. Intergovernmental Panel on Climate Change (IPCC). *IPCC Workshop on Regional Climate Projections and their Use in Impacts and Risk Analysis Studies*; Stocker, T.F., Qin, D., Plattner, G.-K., Tignor, M., Eds.; IPCC Working Group I Technical Support: Bern, Switzerland, 2015.
18. Ruol, P.; Martinelli, L.; Favaretto, C. Vulnerability analysis of the Venetian littoral and adopted mitigation strategy. *Water* **2018**, *10*, 984. [CrossRef]
19. Capolupo, A.; Monterisi, C.; Saponieri, A.; Addona, F.; Damiani, L.; Archetti, R.; Tarantino, E. An Interactive WebGIS Framework for Coastal Erosion Risk Management. *J. Mar. Sci. Eng.* **2021**, *9*, 567. [CrossRef]
20. Pasquali, D.; Marucci, A. The effects of urban and economic development on coastal zone management. *Sustainability* **2021**, *13*, 6071. [CrossRef]
21. Minervino Amodio, A.; Di Paola, G.; Rosskopf, C.M. Monitoring Coastal Vulnerability by Using DEMs Based on UAV Spatial Data. *ISPRS Int. J. Geo-Inf.* **2022**, *11*, 155. [CrossRef]
22. Bruno, M.F.; Saponieri, A.; Molfetta, M.G.; Damiani, L. The DPSIR approach for coastal risk assessment under climate change at regional scale: The case of Apulian coast (Italy). *J. Mar. Sci. Eng.* **2020**, *8*, 531. [CrossRef]

23. Cavaleri, L.; Bajo, M.; Barbariol, F.; Bastianini, M.; Benetazzo, A.; Bertotti, L.; Chiggiato, J.; Davolio, S.; Ferrarina, C.; Magnusson, L.; et al. The October 29, 2018 storm in Northern Italy–an exceptional event and its modeling. *Prog. Oceanogr.* **2019**, *178*, 102178. [CrossRef]
24. Cavaleri, L.; Bajo, M.; Barbariol, F.; Bastianini, M.; Benetazzo, A.; Bertotti, L.; Chiggiato, J.; Ferrarin, C.; Trincardi, F.; Umgiesser, G. The 2019 flooding of Venice and its implications for future predictions. *Oceanography* **2020**, *33*, 42–49. [CrossRef]
25. Rockel, B.; Will, A.; Hense, A. The Regional Climate Model COSMO-CLM (CCLM). *Meteorol. Z.* **2008**, *17*, 347–348. [CrossRef]
26. Intergovernmental Panel on Climate Change (IPCC). Climate Change 2021: The Physical Science Basis. In *Contribution of Working Group I to the Sixth Assessment Report of the Intergovernmental Panel on Climate Change*; Masson-Delmotte, V., Zhai, P., Pirani, A., Connors, S.L., Péan, C., Berger, S., Caud, N., Chen, Y., Goldfarb, L., Gomis, M.I., et al., Eds.; Cambridge University Press: Cambridge, UK; New York, NY, USA, 2021.
27. Schwalm, C.R.; Glendon, S.; Duffy, P.B. RCP8. 5 tracks cumulative CO_2 emissions. *Proc. Natl. Acad. Sci. USA* **2020**, *117*, 19656–19657. [CrossRef] [PubMed]
28. Wood, A.W.; Leung, L.R.; Sridhar, V.; Lettenmaier, D.P. Hydrologic Implications of Dynamical and Statistical Approaches to Downscaling Climate Model Outputs. *Clim. Chang.* **2004**, *62*, 189–216. [CrossRef]
29. Tolman, H.L. *User Manual and System Documentation of WAVEWATCH-III, version 3.14*; Environmental Modeling Center Marine Modeling and Analysis Branch Research Court: College Park, MD, USA, 2009.
30. MedECC. *Climate and Environmental Change in the Mediterranean Basin—Current Situation and Risks for the Future*; First Mediterranean Assessment Report; Cramer, W., Guiot, J., Marini, K., Eds.; Union for the Mediterranean, Plan Bleu, UNEP/MAP: Marseille, France, 2020; 632p.
31. Ferreira, A.; De Haan, L. On the block maxima method in extreme value theory: PWM estimators. *Ann. Stat.* **2015**, *43*, 276–298.
32. Gumbel, E.J. *Statistics of Extremes*; Columbia University Press: New York, NY, USA, 1958; 201p. [CrossRef]
33. US Army Corps of Engineers. *Shore Protection Manual*; Coastal Engineering Research Centre, Government Printing Office: Washington, DC, USA, 1984.
34. Zanuttigh, B.; Palma, G.; Brizzi, G.; Bellotti, G.; Romano, A.; Suffredini, R. Design of a multi-use marine area off-shore the Mediterranean Sea. *Ocean Eng.* **2021**, *221*, 108515. [CrossRef]
35. Canestrelli, P.; Mandich, M.; Pirazzoli, P.A.; Tomasin, A. *Wind, Depression and Seiches: Tidal Perturbations in Venice (1951–2000)*; Centro Previsioni e Segnalazioni Maree: Venezia, Italy, 2001; pp. 1–104.
36. Toimil, A.; Camus, P.; Losada, I.J.; Le Cozannet, G.; Nicholls, R.J.; Idier, D.; Maspataud, A. Climate change-driven coastal erosion modelling in temperate sandy beaches: Methods and uncertainty treatment. *Earth-Sci. Rev.* **2020**, *202*, 103110. [CrossRef]
37. Hurdle, D.P.; Stive, R.J.H. Revision of SPM 1984 wave hindcast model to avoid inconsistencies in engineering applications. *Coast. Eng.* **1989**, *12*, 339–351. [CrossRef]